Hot Electron and Ion Spectra in Axial and Transverse Laser Irradiation in the GXII-LFEX Direct Fast Ignition Experiment[*]

Tetsuo OZAKI, Yuki ABE[1], Yasunobu ARIKAWA[1], Shinichirou OKIHARA[2], Eisuke MIURA[3],
Atsushi SUNAHARA[4], Katsuhiro ISHII[2], Ryohei HANAYAMA[2], Osamu KOMEDA[5],
Yasuhiko SENTOKU[1], Akifumi IWAMOTO, Hitoshi SAKAGAMI, Tomoyuki JOHZAKI[6],
Junji KAWANAKA[1], Shigeki TOKITA[1], Noriaki MIYANAGA[1], Takahisa JITSUNO[1],
Yoshiki NAKATA[1], Koji TSUBAKIMOTO[1], Yoshitaka MORI[2] and Yoneyoshi KITAGAWA[2]

National Institute for Fusion Science, Toki 509-5292, Japan
[1]*Institute of Laser Engineering, Osaka University, Suita 565-0871, Japan*
[2]*The Graduate School for the Creation of New Photonics Industries (GPI), Hamamatsu 431-1202, Japan*
[3]*National Institute of Advanced Industrial Science and Technology, Tsukuba 305-8560, Japan*
[4]*Purdue University, West Lafayette, IN, 47907, United States*
[5]*Advanced Material Engineering Divison, TOYOTA Motor Corporation, Toyota 471-8571, Japan*
[6]*Graduate School of Advanced Science and Engineering, Hiroshima University, Higashihiroshima 739-8527, Japan*

An electron spectrometer was used to measure the electron and ion spectra in two different irradiations of implosion laser to the deuterated spherical shell targets at the direct fast ignition experiments on the Gekko-LFEX facility. In the transverse irradiation against the LFEX laser axis, the low effective hot electron temperature (T_{eff}) and huge neutron yield (Ny) could be obtained although high T_{eff} and low Ny could be observed in the axial irradiation. In the transverse irradiation, the efficient core heating could be obtained because the laser-plasma interaction position is close to the core and the diffusive/ion drag heating may be effective.

1. Introduction

A fast ignition [1–3] is performed by auxiliary heating to the imploded core. Several fast ignition schemes have been studied for decades, such as the electron-driven fast ignition by using spherical target with a cone-attached target. However, the target is complicated, and considerable energy is lost in the cone tip. The hot electrons with divergence are lost because the position of the laser-plasma interaction is far from the core [4]. Therefore, the coupling efficiency is limited. On the other hand, the direct heating method is still studied because the contribution of diffusive heating is found to be large if the hot electron temperature (T_{eff}) can be maintained low. The CANDY fusion reactor, which allows more simple laser structures [5], has been proposed in The Graduate School for the Creation of New Photonics Industries (GPI). The advantage of this method is the simplicity due to the target not only without a guiding cone but also without an external magnetic field [6]. However, in the high-power heating laser, higher T_{eff} caused due to the blow-off plasma accompanying implosion is a serious problem for the coupling efficiency. We try to compare two different types of irradiations and targets. One is the axial irradiation to the spherical shell target for compression, which has a similar configuration to the CANDY. Another type of irradiation is the transverse irradiation to the spherical shell target with two holes [7]. The blow-off plasma from the core irradiated by imploding laser, flows to the heating laser path. Energetic electrons generated by the interaction between the heating laser and the plasma. The target-electron coupling efficiency decreases because the energy is too high. To reduce blow-off plasma, there are holes along the heating laser path. In both cases, the LFEX laser auxiliary heats the compressed core at the maximum compression timing.

2. Experimental Setup

The experiments have been performed using the Gekko XII (GXII)-LFEX [8] laser system in the Institute of Laser Engineering (ILE) in Osaka University. In the axial irradiation, the polystyrene deuteride spherical shell targets are used as shown in Fig. 1. Three beams (250 J/beam 2ω) near LFEX laser (243 - 343 J/total, 1ω) and another three beams in the opposite side are all used as the compression laser. Normal Gaussian shape lasers of 1 ns pulse duration irradiate the target for the compression instead of a tailored

pulse which is used in CANDY-GPI. The polystyrene deuteride spherical shell targets of 500 μmφ, 7 μm-thickness is used. Therefore, T_{eff} increases because the suppression of ablation plasma is not enough when the imploded core is additionally heated by the LFEX.

In the transverse irradiation, six perpendicular beams against LFEX laser axis are used to compress the target. The compression laser pulse is the same as in the axial irradiation. The polystyrene deuteride spherical shell targets of 500 μmφ, 7 μm-thickness with two holes of 100 μmφ along the LFEX axis are used. The invasion of ablation plasma into the LFEX axis can be minimized because there is no shell material on the axis. Therefore, lower $T_{eff.}$ can be expected when the LFEX heats the imploded core. Measurements of the hot electron and ion, and the neutron are conducted using an electron spectrometer (ESM) [9] and a Mandala time-of-flight neutron detection system [10] Three ESMs are installed at 0, 20.9 and 70.5 degrees against the LFEX direction. ESM can measure the electron spectra from 0.5 MeV to 120 MeV and protons or deuterium ions until 7 MeV. There is no mass separation
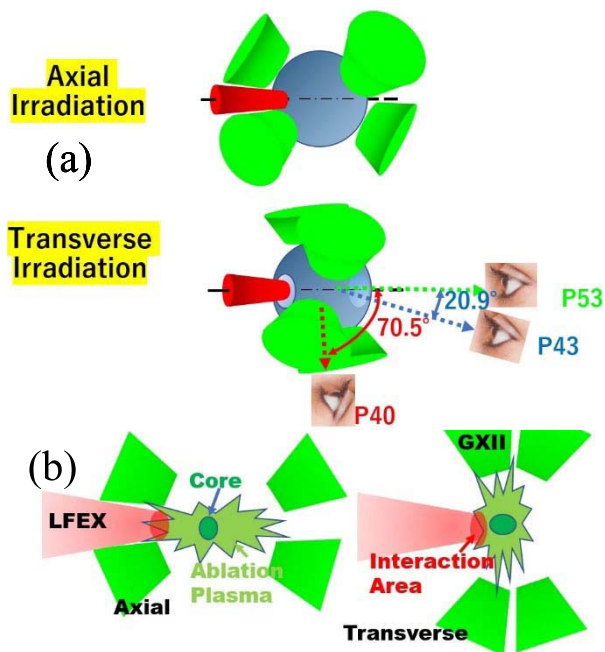

Fig. 1 Target irradiation and ESM arrangement. (a) Arrangements and diagnostics, ESMs are located at 0, 20.9 and 70.5 degrees against LFEX laser axis. 500 μmφ shell and 500 μmφ shell with two 100 μmφ holes are used in the axial and transverse configurations, respectively. Mandala neutron spectrometer is located at the back side against the LFEX direction. (b) Compression and heating phase, The laser irradiations are asymmetry in both cases. Core sides which are directly irradiated by a laser, are strongly ablated. The shapes of the ablation plasmas are also asymmetry. The sides are stronger compressed. Therefore, the precise core shapes in the axial irradiation and in the transverse is slightly pan-cake and sausage shapes [11], respectively.

ability regarding ions in ESM. Here, we assume that the observed ion is mainly deuteron. The experiment was carried out by varying the injection timing of LFEX against GXII shot-by-shot.

3. Experimental Results (Electron)

Figures 2 are the timing dependence of T_{eff} in the axial and transverse configurations, respectively. The timing dependence is the time delay of LFEX laser injection from the peak timing of the GXII laser. In axial irradiation, when the additional heating is earlier than the implosion timing, T_{eff} is relatively low because the influence of the blow-off plasma is small. However, after the implosion timing, the LFEX path is filled with the preformed plasma, T_{eff} increased. +200 ps seems to be near the maximum compression timing from the results of X-ray streak camera (XSC) [11] and Sunahara's simulation [12]. However, T_{eff} is still high. This means that the suppression of the preformed plasma by the GXII is not enough. In the transverse configuration, there is the maximum compression between −200 ps and +300 ps. At +300 ps, still T_{eff} is maintained low although the core seems to be in the expanding phase. At 70 degrees and at any timing in both configurations, T_{eff} are similar because hot electrons emit after trapping by self-electromagnetic field.

We can estimate the electron absorbed energy to the core. The electron deposited energy means the electron drag. The drag is written by Drag = (Laser Energy) × (laser absorption) × (Areal efficiency) × (Deposition). The target areal density (ρR) measurement is performed by the knock-on method [12]. ρRs are 0.019 in the axial configuration and 0.0122 g/cm^2 in transverse configuration, respectively. The energy loss of hot electrons in the core does not strongly depend on each hot electron energy be-
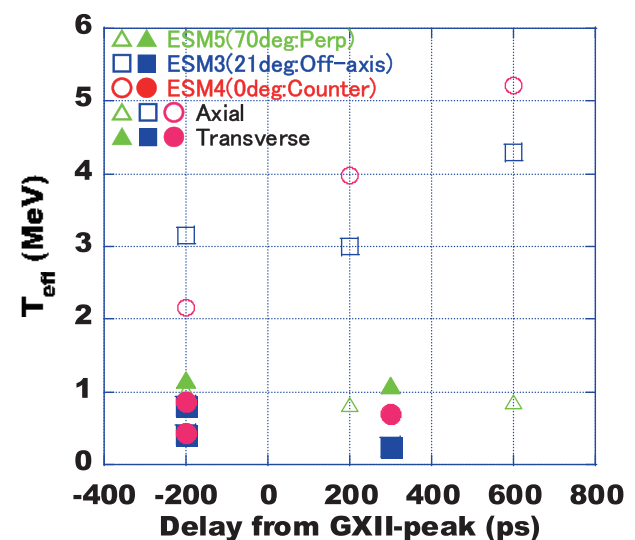

Fig. 2 Electron spectra in the axial and transverse irradiations. $T_{eff.}$ is high due to the blow-off plasma from the target in axial irradiation.

cause ρR is very low compared with the stopping range of the hot electron. The stopping range equivalent energies in the core by the classical process are $E_{SR} = 0.11$ MeV and 0.077 MeV in the axial and transverse configurations, respectively. Therefore, when the hot electron energy of E is greater than E_{SR}, E_{SR} is the deposited energy. If $E < E_{SR}$, E is the deposited energy. The average deposited energy E_{avg} is written by

$$E_{avg} = T_{eff}\left(1 - e^{-\frac{E_{SR}}{T_{eff}}}\right). \qquad (1)$$

Therefore, E_{avg} is estimated to be 0.108 MeV and 0.0736 MeV in the axial and transverse configurations, respectively. Total electron number is calculated by,

$$N_{electron} = \frac{E_{LFEX} \times (1 - R_{ref})}{T_{eff}}, \qquad (2)$$

where the laser reflection R_{ref} of 25 % is assumed [13]. The LFEX input laser energies E_{LFEX} are 262 J and 343 J, respectively. Here, the hot electron beam distribution is also assumed to be ignored in the axial and to be uniform in transverse irradiation. The hot electron deposit energies of 4 ± 1 J and 7 ± 2 J can be obtained from products of E_{avg} and $N_{electron}$ in the axial and transverse configurations, respectively.

4. Experimental Results (Ion and Neutron)

We measure ions spectra by using the same ESMs in electron measurement at the same time. Since ions have a large mass, they are not easily affected by an electromagnetic field formed near the target. According to Sunahara's simulation, the contribution of ion heating in the direct fast ignition is greater than the fast ignition utilized cone guide. The reason is that the ion stopping range is too short and all the ions stop at the cone tip. In the direct fast ignition, the difference of the target ρR strongly reflects the ion spectrum.

The ions are mainly generated by two mechanisms: one is the target normal surface acceleration (TNSA)-like acceleration and another is the ponderomotive acceleration. TNSA-like ions are accelerated by a sheath electric field. TNSA-like ions contain the protons rather than target component deuterons because the electric field extracts the protons adsorbed on target surface. In the ponderomotive acceleration, more deuterons than protons are accelerated, especially in the transverse configuration. Unfortunately, ESM cannot distinguish particle species. The ponderomotive acceleration ions go forward. TNSA-like ions are distributed more uniformly. Therefore, the ions observed at the 70-degree direction are mainly TNSA-like ions and do not change greatly depending on the irradiation timing of the LFEX laser. The ion beam deposition can be obtained from the D-D reaction between the target D and the accelerated beam D because the ponderomotive accelerated

is dominant at 0-degree direction. Thus, if we take into account the ion spectrum at 0 degree, we can obtain the information of the ion loss mechanism.

In the axial configuration, the ion acceleration region is expanded along LFEX laser axis. Therefore, the higher energy ions have been generated. However, the interaction position is far from the core, thus the heating efficiency does not increase due to the ion beam divergence. On the other hand, the ion heating in the transverse configuration can be expected effectively because the interaction position is closed to the core.

The beam-target neutrons are generated because the accelerated deuteron beam hits the deuteride core. Thermal neutrons generated from the core are also generated by the core heating. However, the thermal neutron is hidden behind the beam neutron in many cases because the DD reaction cross section of the energetic beam is too large and the neutron yield is too high. In the axial configuration, we can see the thermal neutron signal [12] when the beam-target neutron is insufficient.

Figure 3 shows the total energy of ions and the neutron yield [14]. Here, energy integration of ion is estimated assuming that ions are spread with the solid angle π (1/4 of the entire space). This assumption of the ion beam divergence is derived from a comparison of three ESMs' ion signals. The total ion energy and the neutron yield (Ny) are normalized by the input energy of LFEX in order to make it easy to compare among shots. Ny in transverse irradiation is 30 times greater than Ny in the axial irradiation. This means that the effect of the beam divergence in the transverse configuration is smaller than that in the axial configuration, because the laser-plasma interaction position is closed to the core in the transverse configuration.

The ions observed at the 0 degree vary greatly depending on the timing because ρRs are also varied by timing. At +200 ps in the axial irradiation, the ion at the 0 degree
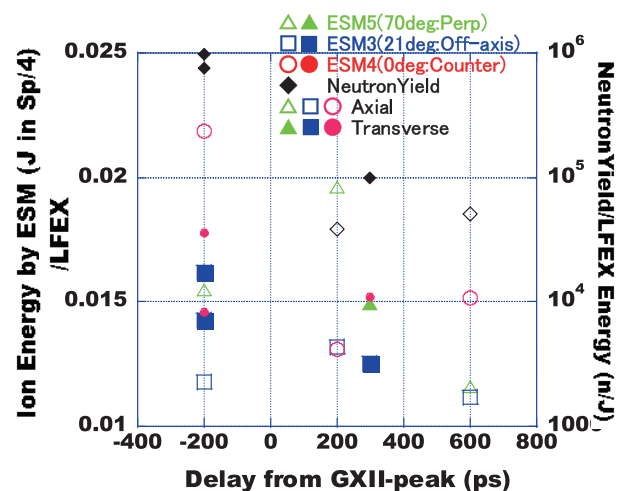

Fig. 3 Timing dependence of observed ion energy and neutron yield. in the axial irradiation. Those values are normalized by the LFEX energy.

decreases sharply. This means that the ion accelerated by the ponderomotive force stops because the core maximum compression occurs around +200 ps. In the transverse irradiation, the timing dependence is not clear from ion measurements because there is no data at the maximum implosion timing. These values are slightly delayed rather than the XSC data and Sunahara's simulation (in both cases at about 0 ps) [15]. The best timing will be made clear by the precise timing dependence experiments. Ion deposit energy is evaluated by multiplication of the ion flux and each ion energy. Here, the ion flux is obtained from neutron yield and target areal density etc. P = (DD-cross section) $\times$ (deuterium density) $\times$ (deuteron range). The ion flux can be obtained by dividing the neutron yield by P. The deposit energies may be approximately 0.6 - 2.5 J in the axial irradiation case.

In this experiment, most of the neutrons seem to come from the beam-target reaction. Therefore, neutron flux can provide deposited ion amount in the core. ρR is measured by a knock-on method [13]. Here, R is determined by an X-ray pinhole camera (XPHC). ρ are estimated to be 2.7 and 1.9 g/cm^3, respectively. T_{eff} (ion) of 0.44 MeV and 0.46 MeV are obtained from the slopes of ion spectra measured by ESM. Ion stopping range is calculated by SRIM code [16]. We can estimate the related target deuteron number. Since Ny (beam) is obtained by Mandala, deposit ion energies of 3 ± 0.5 J in the axial and 17 ± 3 J in the transverse irradiation can be evaluated by the simple calculation, respectively.

Finally, the energy depositions determined by summation the electron (as mentioned in sec. 3) and ion drag heating are 7 ± 1 J in the axial and 24 ± 4 J in the transverse irradiation, respectively. On the other hand, the absorbed energy of 23 ± 3 J in the axial can be expected from X-ray emission measured by XPHC if we assume the black-body radiation and the ion temperature measurement by Mandala. The absorbed energy in the transverse irradiation could not be observed because thermal neutron has been hidden by the huge beam neutron. However, the absorbed energy in the axial irradiation can be expected to be much larger than 23 J considering the increase of the drag heating (7 J to 24 J). The discrepancy between the absorbed energy and drag heating may come from the resistive and the diffusive heating [17].

5. Summary

ESMs are used to compare the electron and ion spectra in two different irradiations of the compression laser. For fast ignition, it is important to suppress preformed plasma (including blow-off from implosion plasma) when the heating laser is injected. The core heating cannot be explained only by the drag heating of electron and ion. The role of the resistive and diffusive heating may be very effective in the direct fast ignition.

Acknowledgements

[1] M. Tabak *et al.*, Phys. Plasmas **1**, 1626 (1994).
[2] Y. Kitagawa *et al.*, Phys. Rev. E **71**, 016403 (2005).
[3] R. Kodama *et al.*, Nature **418**, 933 (2002).
[4] S. Sakata *et al.*, Nature Com. **9**, 3937 (2018).
[5] Y. Kitagawa *et al.*, Plasma Fusion Res. **6**, 1306006 (2011).
[6] S. Fujioka *et al.*, Sci. Rep. **3**, 1170 (2013).
[7] T. Ozaki *et al.*, Physica Scripta **2014**, T161, 014025 (2014).
[8] H. Shiraga *et al.*, Plasma Phys. Control. Fussion **53**, 124029 (2011).
[9] T. Ozaki *et al.*, Rev. Sci. Instrum. **83**, 10D920-1 (2012).
[10] Y. Abe *et al.*, Rev. Sci. Instrum. **89**, 110I114 (2018).
[11] E. Miura *et al.*, HED Phys. **36**, 100890 (2020).
[12] Y. Kitagawa *et al.*, 3P20, IFSA2019.
[13] T. Ozaki *et al.*, J. Phys. **717**, 012043 (2016).
[14] Y. Abe *et al.*, HED Phys. **36**, 100803 (2020).
[15] A. Sunahara *et al.*, J. Phys. **717**(1), 012055 (2016).
[16] http://www.srim.org/
[17] N. Higashi *et al.*, HED Phys. **36** 100829 (2020).